Available online at www.sciencedirect.com
ScienceDirect
Ceramics International 38 (2012) 721–729
CERAMICS INTERNATIONAL
www.elsevier.com/locate/ceramint

Synthesis of porous iron oxide ceramics using Greek wooden templates and mill scale waste for EMI applications

G. Bantsis [a], M. Betsiou [a], A. Bourliva [b], T. Yioultsis [c], C. Sikalidis [a,*]

[a] Department of Chemical Engineering, School of Engineering, Aristotle University of Thessaloniki, 54124 Thessaloniki, Greece
[b] Department of Minerology-Petrology-Economic Geology, School of Geology, Aristotle University of Thessaloniki, 54124 Thessaloniki, Greece
[c] Department of Electrical & Computer Engineering, Aristotle University of Thessaloniki, 54006 Thessaloniki, Greece

Received 11 July 2011; received in revised form 26 July 2011; accepted 27 July 2011
Available online 4th August 2011

Abstract

The scope of this study is the synthesis of low cost iron oxide ceramics with porous structure for lightweight Electromagnetic Interference (EMI) shielding applications, using mill scale waste as the initial material, utilizing Greek wood templates. These wood-templated iron oxide (Fe_2O_3) ceramics were prepared by impregnation of inorganic precursor solution, derivated from mill scale waste, into four different kinds of Greek native wood templates; pine, fir, poplar and beech, followed by thermal treatment.

Scanning Electron Microscopy (SEM) was used to investigate the microstructure of the prepared wood-templated iron oxide specimens. Their iron and oxygen contents were validated by Scanning Electron Microscopy–Energy-Dispersive X-ray Spectroscopy (SEM–EDX) and their mineralogical composition by X-ray Powder Diffractometry (XRD). The wooden substances were found to be completely removed and the synthesized Fe_2O_3 (hematite) was confirmed by XRD, as a single phase. It is also demonstrated that the structures of the iron oxide were hierarchically porous developed according to the wood templates. Moreover, the pore shape and size distribution showed a dependence on the calcination temperature and wood template. Specifically, the temperature increase from 1000 °C to 1200 °C created larger but less pores in μm scale. Finally these low cost iron oxide ceramics exhibited electrical (mainly) and magnetic properties suitable for electromagnetic shielding applications.

Keywords: A. Firing; B. Porosity; C. Electrical properties; C. Magnetic properties

1. Introduction

Biological materials are organized by hierarchical architecture with exquisite designs at several discrete length scales. The astonishing arrays of structures and a broad range of functions are evolved from millions of years of natural selection. As a consequence, these biological systems possess unique characteristics different from the man-made materials. However, biological materials have some limitations for engineering applications because of their thermolabile constituent. Therefore, combining of the heat-resistant components and biological hierarchical structures together could remedy the performance deficiencies [1]. Furthermore, a biological material such as wood provides an excellent template for the natural hierarchical porous structure. The scales range from millimeter scale of growth ring and vessel pore, via micrometer scale of transverse ray parenchyma and longitudinal tracheid or fiber, to nanometer scale of molecular fiber and cell membrane [2]. Woodceramics are promising new porous materials with large potentiality for a variety of industrial applications.

Woodceramics with controlled porosity can have certain properties such as lower thermal conductivity, lower dielectric constant, enhanced electromagnetic shielding properties and higher surface area than their dense counterparts that make them more favourable for certain applications than the pore free material [3,4]. As a result, porous ceramics are employed for thermal insulation, high-temperature filtration, and catalysis [5,6].

Related to the anatomical structure trees can be classified as hardwoods and as softwoods. Wood is a natural composite with

* Corresponding author at: PO Box 1683, 54006 Thessaloniki, Greece. Tel.: +30 2310 996185; fax: +30 2310 996230.
E-mail address: sikalidi@auth.gr (C. Sikalidis).

0272-8842/$36.00
doi:10.1016/j.ceramint.2011.07.064

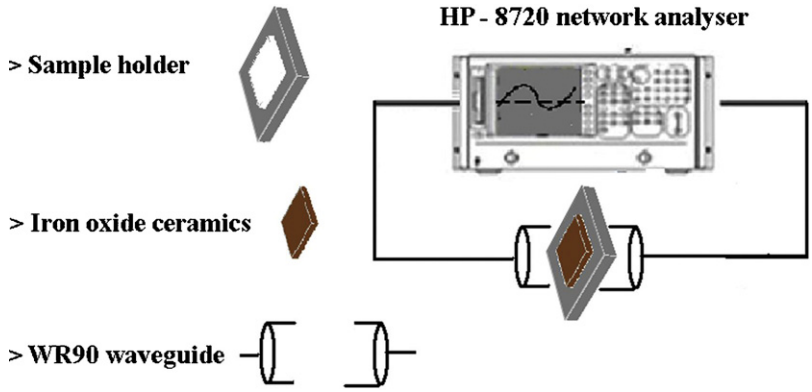

Fig. 1. Schematic presentation of the measurement of electrical and magnetic properties at 8–12 GHz frequency range.

cellulose, hemicellulose and lignin as the major constituents [2]. The morphology and the arrangement of the different cells may vary in a wide range between the different kinds of wood with large vessel cells dominating in hardwood and tracheids dominating in softwood. The diameter of the vessels and tracheids (named as pores) varies between 5 and 50 μm in softwood and between 1 and 300 μm in hardwood. These cells with a preferential orientation in the axial direction offer the possibility of using various infiltration techniques to transform the bioorganic wood structure into an inorganic ceramic material with tailored physical and mechanical properties [7,8].

Several investigations have been focused on the synthesis of biomorphous oxide ceramics. Yermolenko et al. [9] prepared Al_2O_3- and ZrO_2-fibers by oxidizing hydrated cellulose fibers impregnated with solutions of aluminum chloride, zirconium chloride and Al/C and Al/(SiC + C) composites in general [9,10]. Patel and Padhi [11] manufactured TiO_2-fibers by infiltration of natural sisal, jute and hemp fibers with $TiCl_4$. Chakrabarti et al. [12] synthesized cellular SiC ceramics from plant precursor.

Up to now, the technologies for preparing ceramic materials from wood include molten silicon infiltration, reactive infiltration of Si contained vapours, infiltration–pyrolysis of metallic alkoxide, polymeric precursors, sol–gel/carbothermal reduction method, and infiltrating ceramic/oxidation method [2]. However in all prementioned technologies starting materials (besides wooden templates) were rather expensive.

In Greece, there are five plants producing steel, Sidenor, Sovel, Halivourgia Thessalias, Halivourgiki and Elliniki Halivourgia. These plants are spread in North, Central and South Greece [13]. It was estimated that these plants only in the year 2009 had produced over 35,000 tones of steel mill scale waste [14].

Furthermore, there are thousands of trees in Greece with different kinds of woods (hardwood–softwood) and they all contain unique structures. So by making good use of these natural treasures, different metal oxides ceramics with a wide range of pore sizes can be made. The scope of this study is the utilization of mill scale waste for the synthesis of hierarchical iron oxide porous structured ceramics with adequate electrical and magnetic properties for EMI shielding applications using wood templates from four different kinds of Greek native trees (pine, fir, poplar and beech).

2. Materials and methods

2.1. Material preparation

The specimens ($10 \times 10 \times 3$ mm^3) of pine, fir, poplar and beech woods were heated in boiling 5% dilute ammonia for 6 h. By using this extraction procedure one can get rid of the wood extractive compounds, e.g. gums, tropolones, fats and fatty acids, and enhance the connectivity among pores and cellular affinity for the precursor. The extracted wood templates were washed by deionised water and dried at 80 °C for 24 h.

60 g of mill scale waste (<50 μm in particle size) was mixed in 200 ml of conc. H_2SO_4 using a 600 ml glass beaker. The mixture was digested on a hot plate at 100 °C for 30 min followed by the addition of 200 ml of 65% HNO_3. Further heating resulted in a cream white solid substance, which was then heated to dryness. The cream white solid contained iron mainly in the Fe^{3+} form. This soluble in water product (more readily in warm water) was added to a solvent of 500 ml deionised water. Finally suitable quantities of 1 M $NaHCO_3$ solution were added which brought pH values between 6 and 7 (precursor solution) [15,16].

Afterwards, wooden templates were dipped into the precursor solution at 60 °C for 3 days in covered beakers. The complementary precursor solution was added to keep the woods immersed always. After taking out the samples from the solution, they were air dried at 60 °C for another 24 h. Finally, the samples were calcinated at 1000 and 1200 °C for 3 h with a heat rate of 40 °C/h in the atmosphere and air-cooled to room temperature.

2.2. Characterization methods

A Scanning Electron Microscope (JEOL JSM-840) connected to an X-ray Energy Dispersion Spectrometer-EDS (LINK-AN 10000) was employed for the morphological and semi-quantitative chemical characterization of wood-templated iron oxide samples. Furthermore, for the investigation of the complete removal of all wooden components and the transformation to hematite mineralogical analyses of the wood-templated iron oxide samples fired at 1000 and 1200 °C respectively, were performed by using a Philips PW

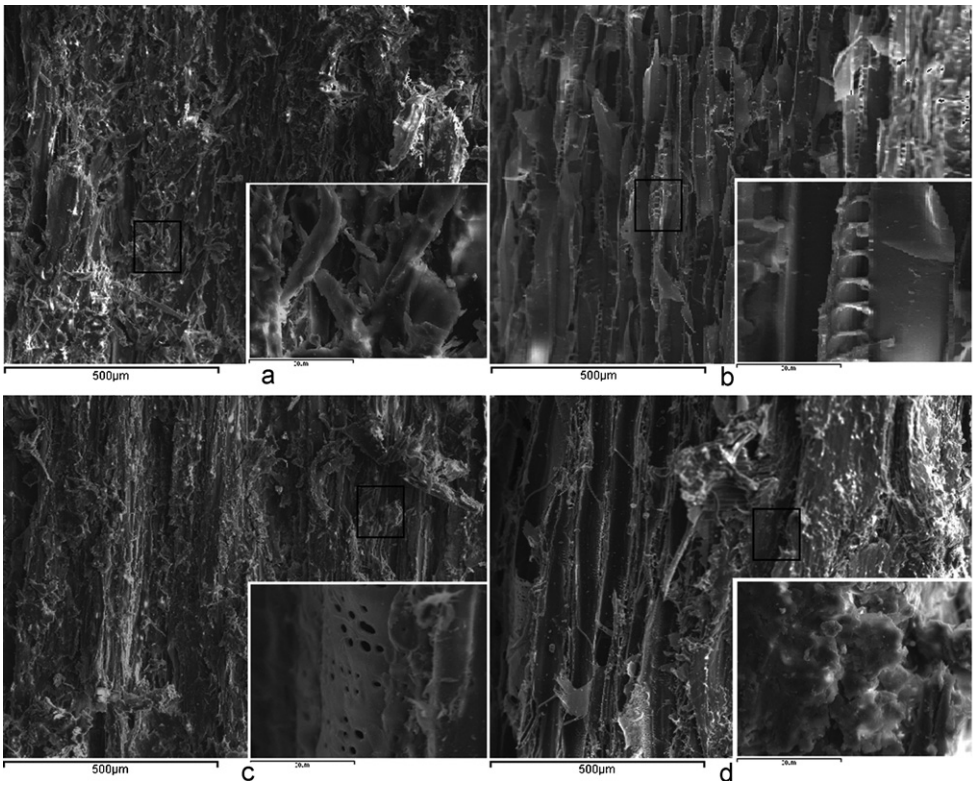

Fig. 2. Micrographic cross sections of 4 wood samples showing the variations in structure between different wood types. (a) Pine, (b) fir (softwoods) and (c) poplar, (d) beech (hardwoods). Insert (a, c and d): hollow channels, pores originated from tracheid cells and vessels respectively. Insert (b): wood arrays.

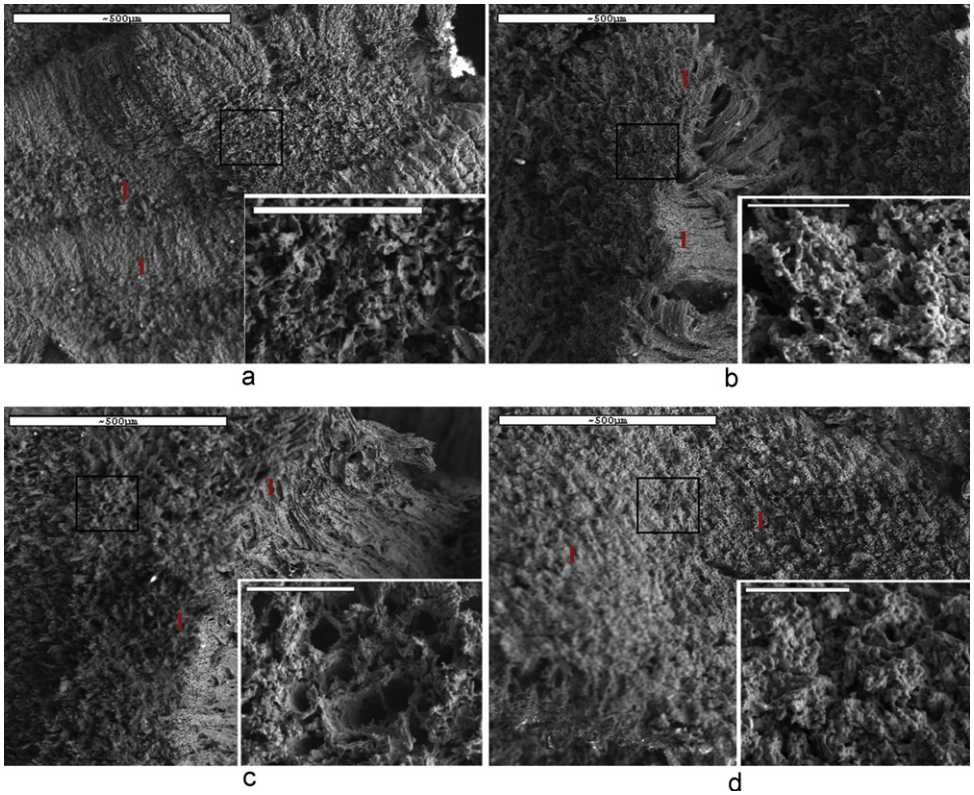

Fig. 3. SEM micrographs of the biomorphous oxide ceramics derived from the 4 woods calcinated at 1200 °C. (a) Pine, (b) fir (softwoods) and (c) poplar, (d) beech (hardwoods). Insert: pore structure of each biomorphous oxide ceramic respectively.

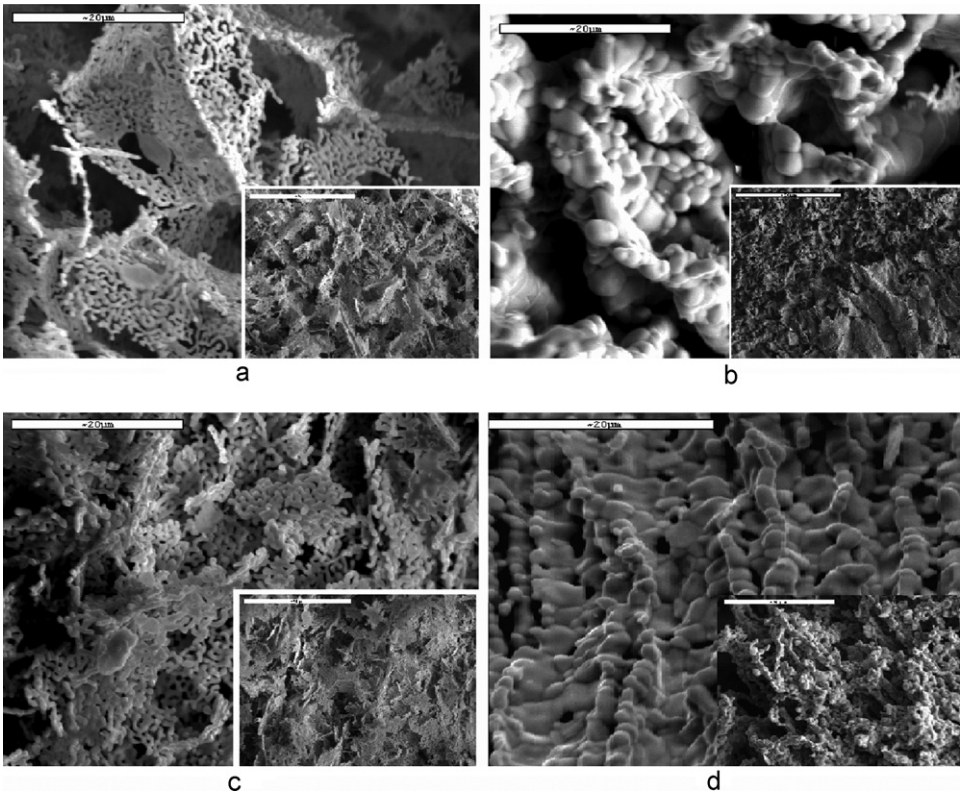

Fig. 4. The crystallite size and morphology of pine (a and b) and fir (c and d) softwood templated Fe_2O_3 bulk samples calcinated at 1000 (a and c) and 1200 °C (b and d) respectively. Insert: larger areas of the same micrographs.

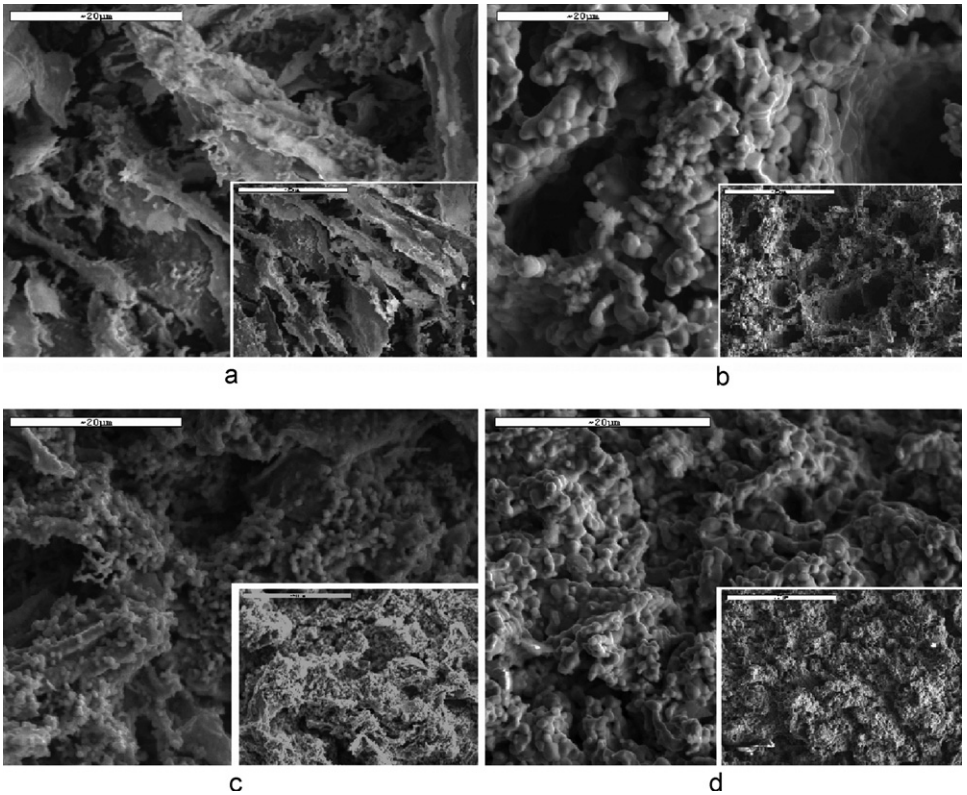

Fig. 5. The crystallite size and morphology of poplar (a and b) and beech (c and d) hardwood templated Fe_2O_3 bulk samples calcinated at 1000 (a and c) and 1200 °C (b and d) respectively. Insert: larger areas of the same micrographs.

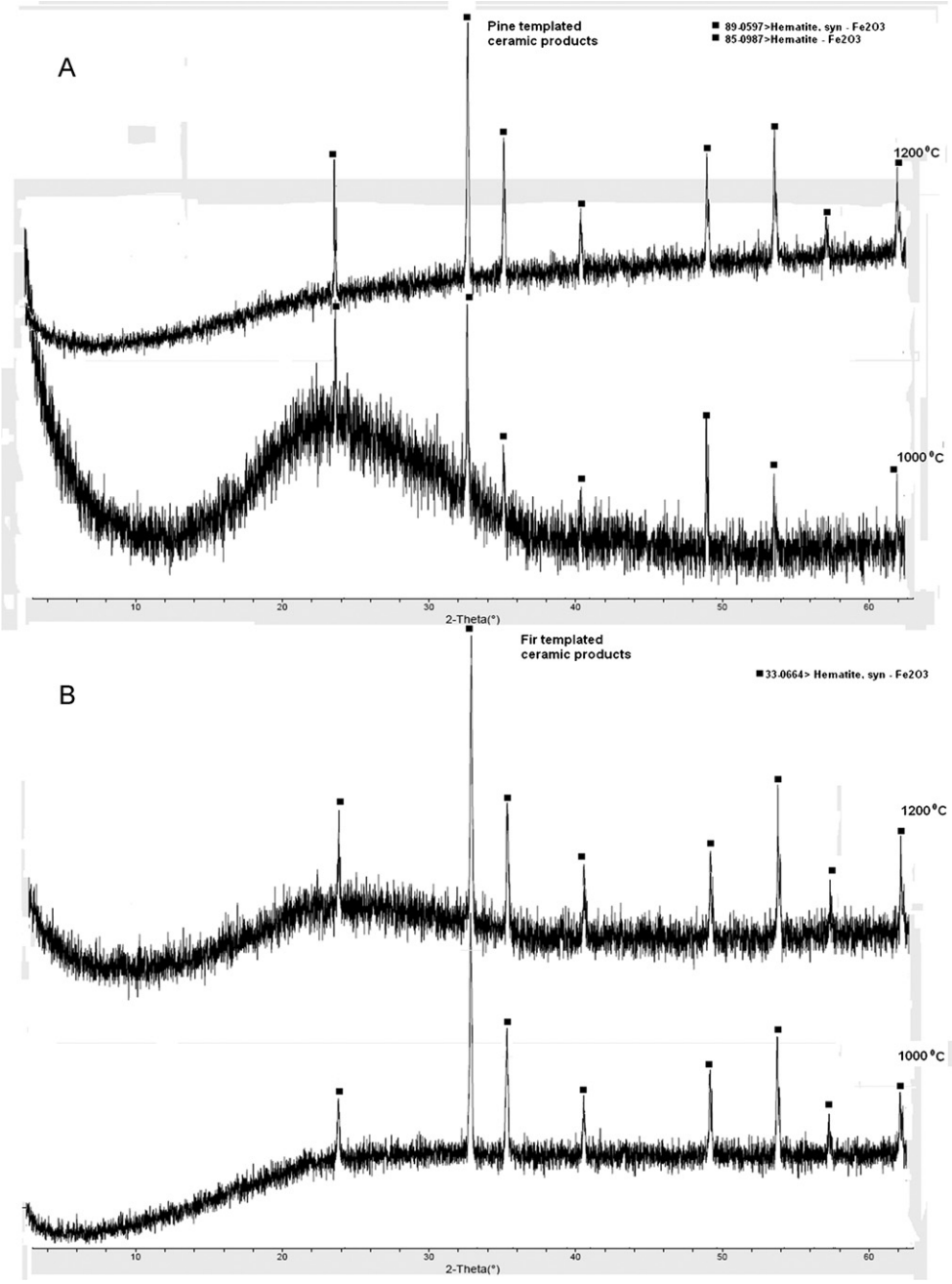

Fig. 6. XRD patterns of wood-templated Fe_2O_3 calcined at 1000 and 1200 °C from (a) pine and (b) fir (softwoods) templates.

1820/00 diffractometer equipped with a PW1710/00 controller. CuKα radiation and a Ni-filter were used. The samples were scanned over an interval of 3–63° 2θ at a scanning speed of 1.2°/min. Finally, measurements of electrical and magnetic properties have been performed by measuring reflection and transmission properties of the iron oxide ceramics with the aid of a Hewlett-Packard HP-8720 (50 MHz–20 GHz) network analyzer (Fig. 1). Each iron oxide ceramic sample was placed in a small WR90 waveguide part of length equal to 3.75 mm and a cross-section of 22.86×10.16 mm^2. Using TRM calibration, the S-parameters (reflection and transmission coefficients) of the samples have been measured (both amplitude and phase). Finally, the analytical expressions relating the S-parameter matrix to the unknown material properties [17] have been inverted to provide estimates of the complex relative dielectric permittivity and magnetic permeability and also the electric and magnetic loss tangents.

3. Results and discussion

3.1. Background data for mill scale waste composition

Mill scale waste chemical, mineralogical and thermogravimetric analyses are thoroughly investigated in previous study [18]. Iron found to dominate in ms, which is common in these types of wastes. The sum of iron oxides in all samples exceeds 96 wt%. Main phases identified within mill scale were found to

be FeO and Fe_3O_4. TG analysis of mill scale presented a small weight increase of 2% due to partial oxidation of magnetite–wursite mixture to hematite (above 550 °C), although the oxidation of pure magnetite leads to a weight gain of 3.455%. Furthermore, the low-temperature oxidation of magnetite particles did not occur, due to the impure magnetite and its large particle size.

3.2. SEM–EDX results

The SEM micrographs of the inheritance structures of the wooden templates (2 softwoods and 2 hardwoods) were first investigated (Fig. 2). As shown in Fig. 2a insert, the microstructure of pine shows hollow channels of nearly same diameter that originate from tracheid cells while in Fig. 2b insert the microstructure of fir shows the existence of wood rays (strips of short horizontal cells that extend in a radial direction and serve to store food and distribute it horizontally). On the contrary the hardwoods, poplar and beech respectively (Fig. 2c and d) have specialized structures called vessels for conducting sap vertically, which on the end grain appear as holes or pores [19].

Due to the decomposition of the biopolymers in the wooden templates during pyrolysis and the burn out of the carbon during sintering, large shrinkages have been found in all samples. The shrinkage exhibited an anisotropic behaviour for all 4 samples. Fig. 3 shows the cellular microstructure of the

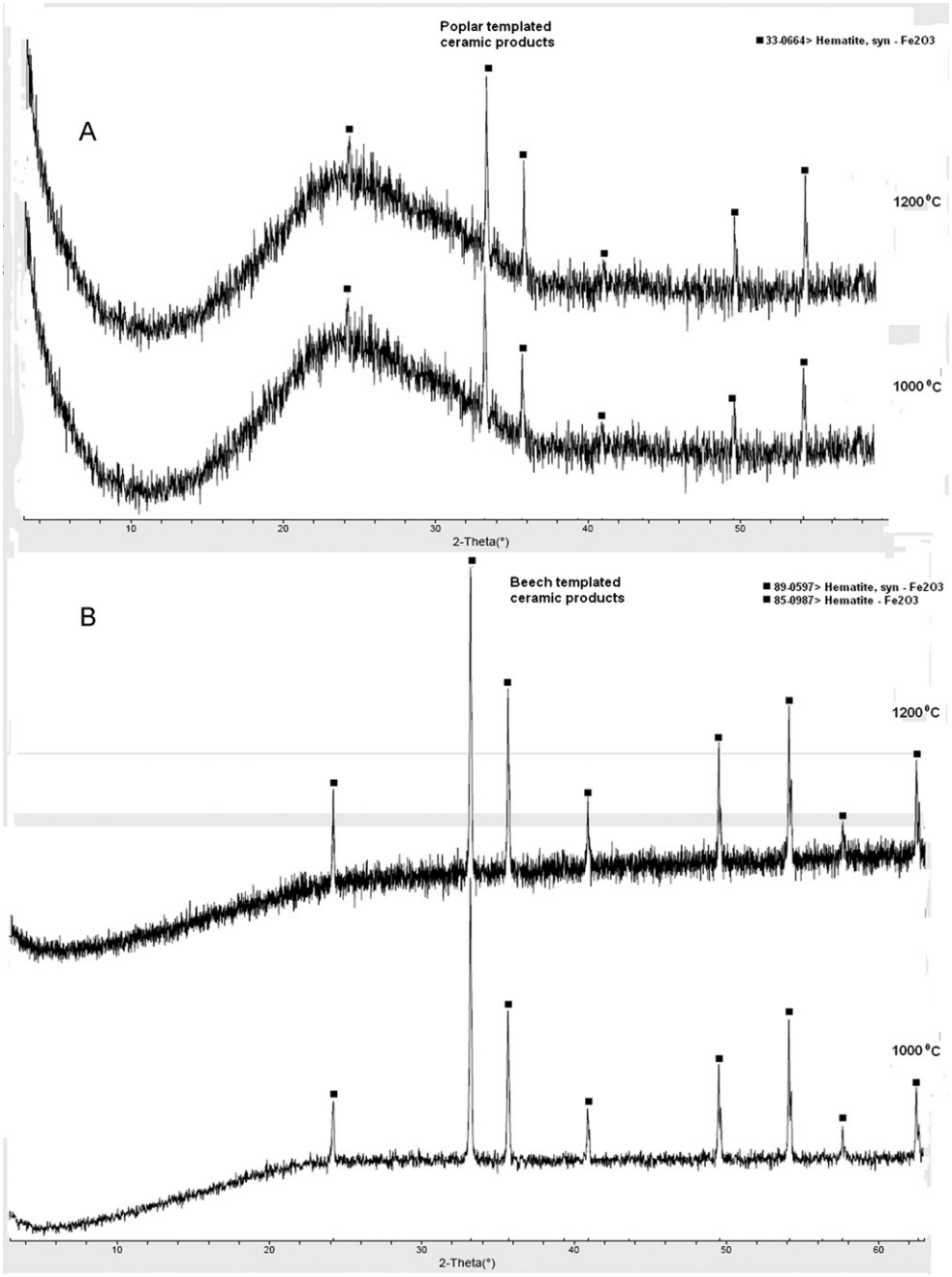

Fig. 7. XRD patterns of wood-templated Fe_2O_3 calcined at 1000 and 1200 °C from (a) poplar and (b) beech (hardwoods) templates.

biomorphous oxide ceramics derived from the 4 woods in axial direction calcinated at 1200 °C. As may be seen, the initial cellular anatomy is not fully reproduced to the similar ceramic products. Better shaped micropores are presented in poplar and pine (softwood–hardwood, Fig. 3c and a) while in beech (hardwood) and especially in fir (softwood) the size distribution of micropores is larger although these micropores are more random oriented and shaped (Fig. 3d and b). Furthermore, EDX study (Fig. 3) showed that in all scanned areas from the 4 woods calcinated at 1200 °C, Fe and O_2 dominate (I). The above supports the possible presence of iron oxides in these areas although a full estimation is given through XRD results.

The influence of calcination temperature on the crystallite size and morphology in general of wooden templated Fe_2O_3 bulk samples is shown in Figs. 4 and 5. Fig. 4 shows the crystallite size and morphology of pine (a and b) and fir (c and d) softwood templated Fe_2O_3 bulk samples calcinated at 1000 (a and c) and 1200 °C (b and d) while in Fig. 5 the crystallite size and morphology of poplar (a and b) and beech (c and d) hardwood templated Fe_2O_3 bulk samples calcinated at 1000 (a and c) and 1200 °C (b and d) are shown respectively. In both figures crystallite size is induced by sintering and ripening as calcinated temperature is raised. Especially, in Fig. 4 the characteristics of softwood cells are clearly transformed from flake structure (1000 °C, Fig. 4a and c) to a more scale structure (1200 °C, Fig. 4b and d) although the same phenomenon is also presented in Fig. 5 (hardwoods). In addition, many small pores on the walls of the wooden templated Fe_2O_3 bulk samples were created by the thermal contraction of tracheid and vessel cells. The anisotropic thermal contraction of the iron oxide wall at 1000 °C causes parts of cell wall to rupture and bring about these new pores [20]. The formation and assembly of wood-templated Fe_2O_3 are under the direction of biotemplate's morphology and the calcination temperature.

3.3. XRD results

In order to validate the development of Fe_2O_3, the samples were pulverized for powder X-ray diffraction. In Figs. 6 and 7 XRD patterns of all the samples from different wood templates and calcination temperatures are illustrated. According to these patterns, the original components of wood are removed completely and the Fe_2O_3 is confirmed as the single phase. When the temperature rises, the peaks in the XRD pattern from

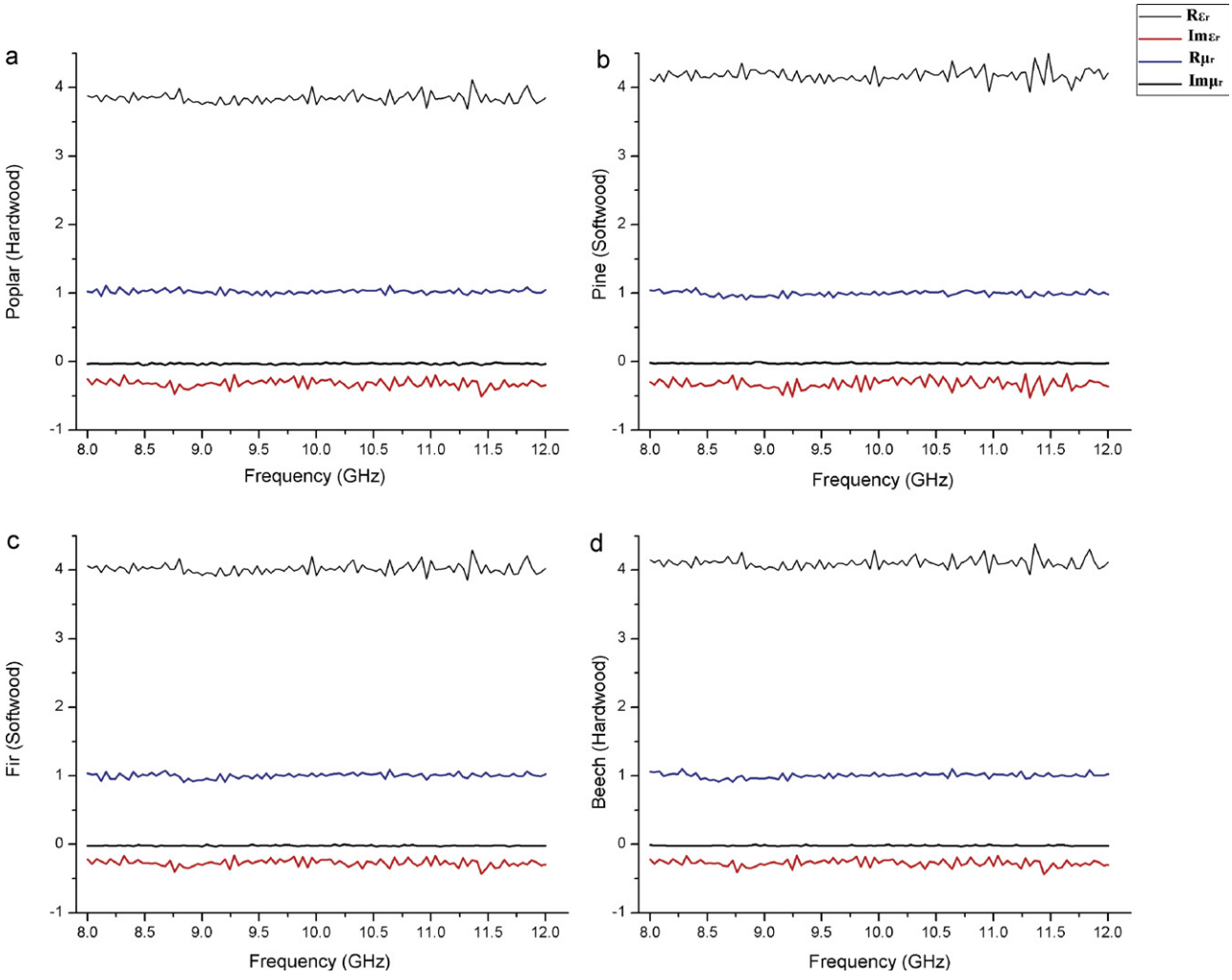

Fig. 8. Measurement of electric and magnetic properties at 8–12 GHz frequency range of poplar and beech (a and d)–pine and fir (b and c) hardwood–softwood templated Fe_2O_3 bulk samples calcinated at 1200 °C.

Table 1
Average values of electric, magnetic properties and loss tangents at 8–12 GHz frequency range of poplar and beech, and pine and fir hardwood–softwood templated Fe_2O_3 bulk samples calcinated at 1200 °C.

Greek woods	Electric properties		Magnetic properties		Loss tangents	
	$\mathrm{Re}\{\varepsilon_r\}$	$\mathrm{Im}\{\varepsilon_r\}$	$\mathrm{Re}\{\mu_r\}$	$\mathrm{Im}\{\mu_r\}$	$\tan\delta_e$	$\tan\delta_m$
Poplar	3.843	−0.313	1.0236	−0.0292	0.081	0.0285
Pine	4.175	−0.321	0.9973	−0.0228	0.077	0.0229
Fir	4.019	−0.271	1.0008	−0.0181	0.067	0.0181
Beech	4.104	−0.272	1.0035	−0.0175	0.066	0.0174

the same wood template become somewhat sharper and more intense. Higher temperature leads to the increase in the size of the Fe_2O_3 crystallites.

3.4. Electric and magnetic properties

Electromagnetic shielding – absorbing materials (in this case iron oxide ceramics with porous structure) can be divided into three types as electric loss, magnetic loss and dielectric loss materials [21–23].

In general the accuracy of the measurement of electric and magnetic properties in materials originated form wastes, is limited due to impurity, large particle size distribution and inhomogeneity of the wastes. This is particularly the case for the measurements of low values of the imaginary parts of complex electric and magnetic properties and the associated loss tangents. However, there is a strong indication for an electric conductivity appropriate enough for making these materials suitable for lightweight EMI shielding applications (in X-band frequency range) in all samples and an almost zero magnetic conductivity in most cases. Specifically, as presented in Fig. 8 and Table 1 average electric loss tangent ($\tan\delta_e$) for Beech is 0.066 while for poplar reaches 0.081, where $\delta = 1/\sqrt{\pi f \mu \sigma}$ is the skin depth (m), f the radiation frequency (Hz), μ the magnetic permeability of the conductor (H/m) and σ the electrical conductivity of the material ($\Omega^{-1}\,\mathrm{m}^{-1}$). The smaller the skin depth, the better the shielding capacity [24].

Materials with such relative high electric loss tangent ($\tan\delta_e$) reduce electromagnetic radiation while electromagnetic energy is mainly attenuated as a resistor. Furthermore magnetic loss tangent for beech is 0.0174 while for poplar reaches 0.0285, values that indicate almost zero electromagnetic reduction (EMI shielding effectiveness in X-band frequency range) from magnetic losses. Finally small increment in $\tan\delta_m$ and especially in $\tan\delta_e$ for different kinds of wooden templates is attributed mainly to the pore structure of each iron oxide ceramic sample. Better shaped micropores in poplar and pine (softwood–hardwood, Fig. 3c and a) form a continuous conduction path (without reaching percolation threshold), therefore a better electric conductivity in all X-band frequency range, while in beech (hardwood) and fir (softwood) this is not the case (Fig. 3d and b).

4. Conclusions

The shape and size of wooden cells have been replaced hierarchically from hematite originated from a precursor solution utilizing mill scale waste. By increasing the calcination temperature from 1000 to 1200 °C porous structures found to be larger in size but fewer in micrometer scale. Furthermore, the porous structure of the iron oxide ceramics that were developed depended mainly on the morphology and the initial porous structure of the native wooden-templates rather than the kind of each native wood (hardwood–softwood). Finally iron oxide ceramics with better porous structure presented electrical properties adequate enough for EMI shielding applications in X-band frequency range.

References

[1] Z. Liu, T. Fan, D. Zhang, X. Gong, J. Xu, Hierarchically porous ZnO with high sensitivity and selectivity to H_2S derived from biotemplates, Sens. Actuators B: Chem. 136 (2008) 499–509.
[2] J. Qian, Z. Jin, Preparation and characterization of porous, biomorphic SiC ceramic with hybrid pore structure, J. Eur. Ceram. Soc. 26 (2006) 1311–1316.
[3] D.J. Green, P. Colombo, Cellular ceramics: intriguing structures, novel properties and innovative applications, Mater. Res. Soc. Bull. 4 (2003) 296–300.
[4] K. Shibata, T. Okabe, K. Saito, T. Okayama, M. Shimada, A. Yamamura, R. Yamamoto, Electromagnetic shielding properties of woodceramics made from wastepaper, J. Porous Mater. 4 (1997) 269–275.
[5] M.E. Davis, Ordered porous materials for emerging applications, Nature 417 (2002) 813–821.
[6] A. Kelly, Why engineer porous materials? Philos. Trans. R. Soc. A 364 (2006) 5–14.
[7] A. Egelja, J. Gulicovski, A. Devečerski, M. Ninić, A. Radosavljević-Mihajlović, B. Matović, Preparation of biomorphic SiC ceramics, Sci. Sintering 40 (2008) 141–145.
[8] V.S. Kiselov, E.N. Kalabukhova, A.A. Sitnikov, P.M. Lytvyn, V.I. Poludin, V.O. Yukhymchuk, A.E. Belyaev, Effect of Si infiltration method on the properties of biomorphous SiC, Semicond. Phys. Quantum Electron. Optoelectron. 12 (2009) 68–71.
[9] I.N. Yermolenko, T.M. Ulyanova, P.A. Vityaz, I.L. Fyodorova, Reactive ceramic fibres, Rev. Int. Hautes Temp. Refract. 23 (1986) 99–104.
[10] X. Zhang, G. Meng, X. Liu, Preparation and characterization of tubular porous ceramics from natural zeolite, J. Porous Mater. 15 (2008) 101–106.
[11] M. Patel, B.K. Padhi, Titania fibres through jute fibre substrates, J. Mater. Sci. Lett. 12 (1993) 1234–1235.
[12] O.P. Chakrabarti, H.S. Maiti, R. Majumbar, Biomimetic synthesis of cellular SiC based ceramics from plant precursor, Bull. Mater. Sci. 27 (2004) 467–470.
[13] G. Bantsis, C. Sikalidis, M. Betsiou, T. Yioultsis, A. Bourliva, Ceramic building materials for electromagnetic interference shielding using metallurgical slags, Adv. Appl. Ceram. 110 (2011) 233–237.
[14] SIDENOR, Personal communication, 2009.
[15] M.A. Legodi, D. Waal, The preparation of magnetite, goethite, hematite and maghemite of pigment quality from mill scale iron waste, Dyes Pigments 74 (2007) 161–168.

[16] Y.-S. Li, The use of waste basic oxygen furnace slag and hydrogen peroxide to degrade 4-chlorophenol, Waste Manage. 19 (1999) 495–502.
[17] D.M. Pozar, Microwave Engineering, second ed., John Wiley & Sons, New York, 1998.
[18] G. Bantsis, C. Sikalidis, M. Betsiou, T. Yioultsis, Th. Xenos, Electromagnetic absorption, reflection and interference shielding in X-band frequency range of low cost ceramic building bricks and sandwich type ceramic tiles using mill scale waste as an admixture, Ceram. Int. (2011), doi:10.1016/j.ceramint.2011.06.010.
[19] S. Mayo, R. Evans, F. Chen, R. Lagerstrom, X-ray phase-contrast microtomography and image analysis of wood microstructure, J. Phys.: Conf. Ser. 186 (2009) 012105.
[20] Z. Liu, T. Fan, W. Zhang, D. Zhang, The synthesis of hierarchical porous iron oxide with wood templates, Micropor. Mesopor. Mater. 85 (2005) 82–88.
[21] L. Olmedol, G. Chateau, C. Deleuzec, J.L. Forveille, Microwave characterization and modelization of magnetic granular materials, J. Appl. Phys. 73 (1993) 6992–6994.
[22] J.Y. Shin, J.H. Oh, The microwave absorbing phenomena of ferrite microwave absorbers, IEEE Trans. Magn. 29 (1993) 3437–3439.
[23] G. Viau, F. Ravel, P. Achier, Preparation and microwave characterization of spherical and monodisperse $Co_{20}Ni_{80}$ particles, J. Appl. Phys. 76 (1994) 6570–6572.
[24] E. Zornoza, G. Catala, F. Jimenez, L. Ga Andion, P. Garces, Electromagnetic interference shielding with Portland cement paste containing carbon materials and processed fly ash, Mater. Construcc. 60 (2010) 21–32.